Croatian Society for Materials Protection

Metalurgija/Metallurgy

Vol. 65 No. 2 / 2026

Hot Deformation Behavior and Constitutive Modeling of C61300 Aluminum Bronze for Gymnastics Equipment Applications

Xue Bai [1] and Yihang Gong [2*]

https://doi.org/10.64486/m.65.2.10

[1] Jiangsu Vocational College of Nursing, Jiangsu, Chine; baixue916@163.com
[2] Dankook University, South Korea; 15232821733@163.com
* Correspondence: 15232821733@163.com

Type of the Paper: *Article*
Received: August 31, 2025
Accepted: December 17, 2025

Abstract: The hot deformation behavior of C61300 aluminum bronze at deformation temperatures of 600 °C – 900 °C and strain rates of 0.001 s^{-1} – 1 s^{-1} was studied by Gleeble-3500 thermo-mechanical simulator. Based on the hot compression test data, true stress–true strain curves of C61300 under different deformation conditions were obtained, and a constitutive equation describing the alloy's hot deformation behavior was established through linear regression. The results show that flow stress decreases with increasing deformation temperature and increases with increasing strain rate.

Keywords: hot deformation behavior, aluminum bronze alloy, constitutive equation, flow stress

1. Introduction

As a core structural component in the support frame of gymnastics mats, the adjustable slide rail is widely used in training equipment such as floor-exercise mats, high- and low-bar auxiliary protection mats, and vault run-up mats. It is the key mechanism that enables flexible adjustment of the height and position of the mat. During operation, the component must withstand the long-term static load of the mat, the transient impact load generated during athlete landings, and the cyclic stresses associated with frequent extension and adjustment. Consequently, its operating environment is complex and the mechanical conditions are severe [1–5].

C61300 is a metallurgical-grade aluminum bronze alloy characterized by high strength and hardness. By optimizing the aluminum content and adding small amounts of iron, nickel, and other strengthening elements, the alloy demonstrates excellent mechanical properties and corrosion resistance. Its typical yield strength exceeds 550 MPa, and its Brinell hardness is above 190 HB, significantly higher than that of conventional brass or carbon steel [6]. The alloy also exhibits excellent deformation resistance and fatigue performance under repeated impact and compression loads. In addition, C61300 shows strong oxidation resistance and electrochemical corrosion resistance in humid and chloride-containing environments, effectively withstanding exposure to sweat, moisture, and common cleaning agents in gyms, thereby reducing the likelihood of fretting wear or surface adhesion caused by corrosion. Proper heat treatment can further improve its surface quality [7–9]. When combined with precision machining, the alloy provides low friction and a smooth fit between the slide guide groove and the slider, enhancing the overall operability of the adjustment mechanism.

C61300 aluminum bronze is a high-performance copper alloy whose chemical composition is presented in Table 1. Its comprehensive performance is achieved through alloying with copper and aluminum as the primary elements, together with appropriate trace additions of iron and nickel [10]. The alloy offers high mechanical strength, hardness, excellent wear resistance, and outstanding fatigue resistance. At the same time, it maintains stable structure and functionality in humid, sweaty, and mildly acidic or alkaline environments. Owing to these properties, C61300 is widely used in demanding applications such as marine propulsion systems, aerospace joints, automotive synchronizer gear rings, and heavy-duty mechanical transmission components [11–15].

Table 1. Chemical composition (mass fraction / %) of C61300 aluminum bronze

Element	Cu	Al	Fe	Ni	Mn	Zn	Other impurities
Content / wt.%	balance	9.0–11	3.0–5.0	⩽0.5	⩽0.5	⩽0.2	—

In gymnastics training equipment, the mechanical and corrosion properties of C61300 aluminum bronze provide reliable support for the adjustable slide-rail system. Its high fatigue resistance prevents the initiation of micro-cracks or structural degradation under long-term cyclic impact loads generated by repetitive athletic movements. The alloy's excellent wear resistance limits surface damage and dimensional changes caused by frequent sliding adjustments, thereby maintaining smooth operation and positioning accuracy [16–18]. In addition, its good thermal conductivity facilitates rapid dissipation of friction-induced heat, reducing the risk of sticking or operational instability due to local temperature rise.

The use of C61300 aluminum bronze in the slide-rail assembly enhances the structural rigidity and dynamic stability of the support frame. A reliable adjustment mechanism ensures consistent alignment and secure load transfer during repeated use, reducing the likelihood of equipment malfunction such as unintended slippage, support instability, or locking failure [19]. These performance characteristics are essential for ensuring operational safety and long-term durability under high-intensity training conditions [20–23].

To meet the requirements of sliding stability, fatigue resistance, and manufacturing adaptability for the adjustable slide-rail of the gymnastics cushion support frame, C61300 aluminum bronze was selected as the structural material. In this study, hot-compression tests of C61300 aluminum bronze were conducted at different temperatures and strain rates using a Gleeble-3500 thermal-simulation machine. The plastic-flow behavior and microstructural evolution under hot-deformation conditions were analyzed, and a constitutive equation describing the alloy's high-temperature deformation behavior was established. These results provide a basis for optimizing the hot-extrusion process parameters and improving the overall performance of components manufactured from C61300 aluminum bronze.

2. Hot compression test of C61300 aluminum bronze

The experimental material used in this study was C61300 aluminum bronze, whose main alloying elements are Cu, Al, Fe, and Ni. The chemical composition of the alloy is shown in Table 2. C61300 exhibits good strength and hot workability and can be further strengthened through appropriate heat treatment. During non-equilibrium solidification, the alloy forms a dendritic solid-solution matrix, and a small amount of black eutectic phases can be observed between the dendrites.

The cast ingot was homogenized at 900 °C and then machined into cylindrical specimens. Isothermal, constant-strain-rate compression tests were conducted on a Gleeble-3500 thermal-simulation testing machine. The specimens were heated to the target deformation temperature at a rate of 4 °C/s, held for 1 min to ensure thermal equilibrium, and then compressed to the desired strain. The data-acquisition system automatically recorded and corrected the experimental measurements and provided the true-stress–true-strain data.

The deformation temperatures used in the tests were 600 °C, 700 °C, 800 °C, and 900 °C, while the strain rates were 0.001 s^{-1}, 0.01 s^{-1}, 0.1 s^{-1}, and 1 s^{-1}. Immediately after deformation, the specimens were water-quenched to preserve the microstructure. The test parameters are summarized in Table 2.

https://doi.org/10.64486/m.65.2.10

Table 2. Chemical composition (mass fraction / %) of the aluminum bronze alloy used in this study

Element	Cu	Al	Fe	Ni	Mn	Zn
Content / wt.%	balance	10.5	4.73	4.66	0.085	0.015

Table 3. Processing parameters of specimens prior to hot compression testing

Parameter	Soaking time min	Heating rate ℃/s	Testing temperature ℃	Strain rate s^{-1}	Total true strain %
	1	4	600–900	0.001–0.1	50

3. Experimental data and constitutive modelling

The true stress–true strain curves of C61300 aluminum bronze obtained from the hot-compression tests are shown in Fig. 1. During testing, friction between the specimen and anvils must be considered: when the strain exceeds 0.6, friction-induced constraints cause significant deviations in the measured flow stress, making the corresponding part of the curve unreliable. In evaluating the high-temperature deformation behavior of aluminum bronze, test parameters such as deformation temperature, strain rate, work-hardening response, and dynamic-recrystallization characteristics were systematically varied [24]. The results indicate that dynamic recrystallization occurs only under specific combinations of temperature and strain rate. This is reflected in the stress–strain curves, where the flow stress reaches a peak and subsequently levels off. Conditions that promote dynamic recrystallization include higher deformation temperatures or lower strain rates.

The true stress–strain curves obtained from the Gleeble tests show that flow stress increases with strain due to work hardening, and stabilizes after reaching a peak value as dynamic softening becomes dominant. When the deformation temperature increases at a constant strain rate, the flow-stress level decreases correspondingly. The results further show that, at a fixed temperature, the flow stress increases with strain rate. For strain rates between 0.1 s^{-1} and 1 s^{-1}, the curves exhibit a clear peak followed by a decline, which is associated with dynamic softening processes such as dynamic recovery and dynamic recrystallization, as well as localized flow phenomena.

At strain rates of 0.01 s^{-1} and 1 s^{-1}, the thermoplastic flow behavior is strongly influenced by the evolution of dislocation structures within the material. During the early stages of deformation, significant energy is required for dislocation nucleation. Once the flow stress reaches its peak and approaches a steady state, the deformation behavior is governed by the balance between dislocation generation, rearrangement, and annihilation. Under these conditions, dynamic recovery is the dominant mechanism. In this steady-state regime, key microstructural parameters remain nearly constant, including the average subgrain size, the internal misorientation, and the dislocation density.

At a strain rate of 0.1 s^{-1}, the stress–strain response becomes more complex than under recovery-dominated conditions, and a similar trend is observed at 1 s^{-1}. After the peak stress is reached, the flow curve exhibits a softening region followed by a plateau. When the stacking-fault energy (SFE) of the alloy is relatively low, the width of extended dislocations increases, and the resulting dislocation network restricts dislocation mobility. In this case, recovery mechanisms such as cross-slip and climb are inhibited, reducing the rate of substructure refinement. Although the dislocation density remains high, dislocation tangles form along subgrain boundaries, producing a refined subgrain structure. Under the combined influence of stress, deformation temperature, and accumulated strain, dynamic recrystallization (DRX) is initiated, which is manifested by the peak and subsequent softening behavior observed on the stress–strain curve.

https://doi.org/10.64486/m.65.2.10

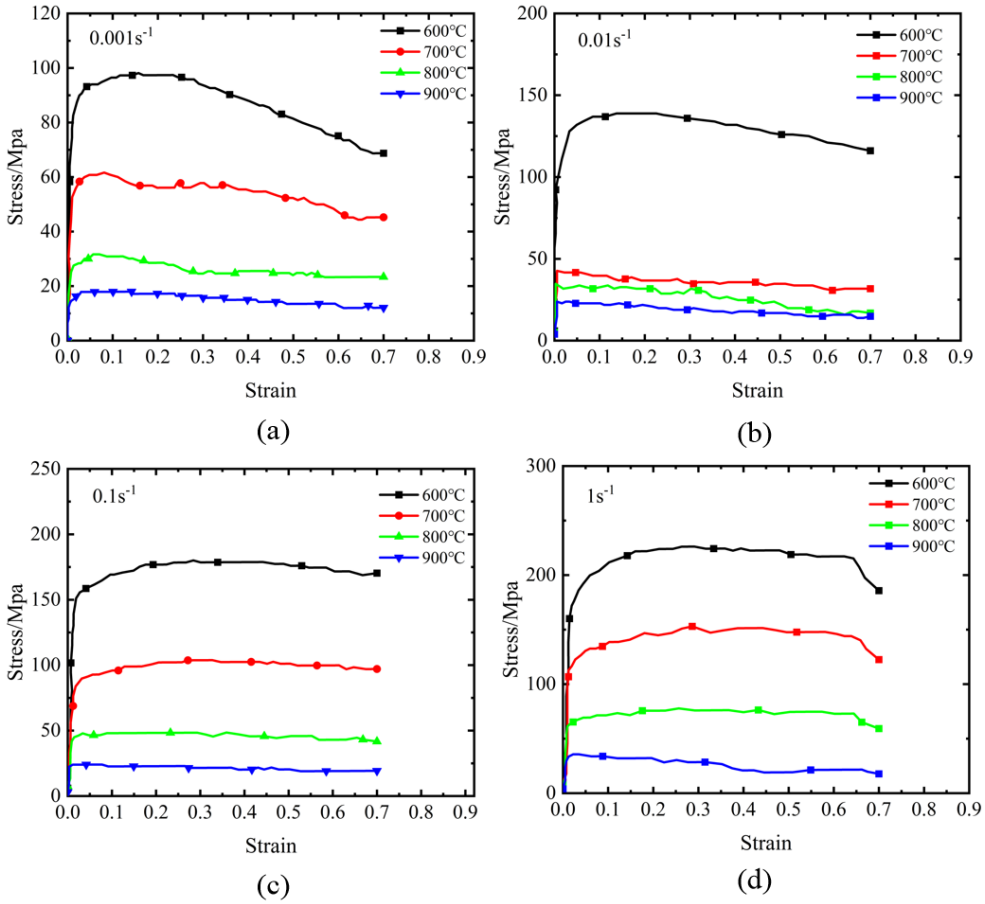

(a) 0.001 s^{-1}; (b) 0.01 s^{-1}; (c) 0.1 s^{-1}; (d) 1 s^{-1};

Figure 1. True stress–true strain curves at different strain rates

Under high-temperature plastic deformation conditions of C61300 aluminum bronze, the relationship between true stress, strain, strain rate, and temperature can be described by the Arrhenius-type constitutive model. The Arrhenius equations are expressed as follows:

$$\dot{\varepsilon} = A_1\sigma^{n_1}\exp(\frac{-Q}{RT}), \quad \alpha\sigma \le 0.8 \tag{1}$$

$$\dot{\varepsilon} = A_2\exp(\beta\sigma)\exp(\frac{-Q}{RT}), \quad \alpha\sigma \ge 1.2 \tag{2}$$

$$\dot{\varepsilon} = A[\sinh(\alpha\sigma)]^n\exp(\frac{-Q}{RT}), \quad \text{for all } \sigma \tag{3}$$

where: R is the molar gas constant (8.314 J·mol^{-1}·K^{-1}, σ is the stress, MPa, Q is the apparent activation energy of thermal deformation（J/mol）, A, A_1, A_2, α, β, n and n_1 are temperature-independent material constants. Here, $\alpha = \beta / n_1$. T represents the deformation temperature in kelvin (K). According to the Arrhenius model, the strain rate during high-temperature plastic deformation is governed by a thermally activated process. Therefore, the relationship among strain rate, temperature, and flow stress can be expressed using the Zener–Hollomon parameter Z:

$$Z = \dot{\varepsilon}\exp\left(\frac{Q}{RT}\right) = A\left[\sinh\left(\alpha\sigma\right)\right]^n \tag{4}$$

When the temperature T is constant, the parameters Q, A, R, and n are constants. Taking the natural logarithm of both sides of Eqs. (1) and (2), the slopes corresponding to n and β can be obtained:

$$In\dot{\varepsilon} = InA_1 + n_1In\sigma - \frac{Q}{RT} \tag{5}$$

https://doi.org/10.64486/m.65.2.10

$$In\dot{\varepsilon} = InA_2 + \beta\sigma - \frac{Q}{RT} \tag{6}$$

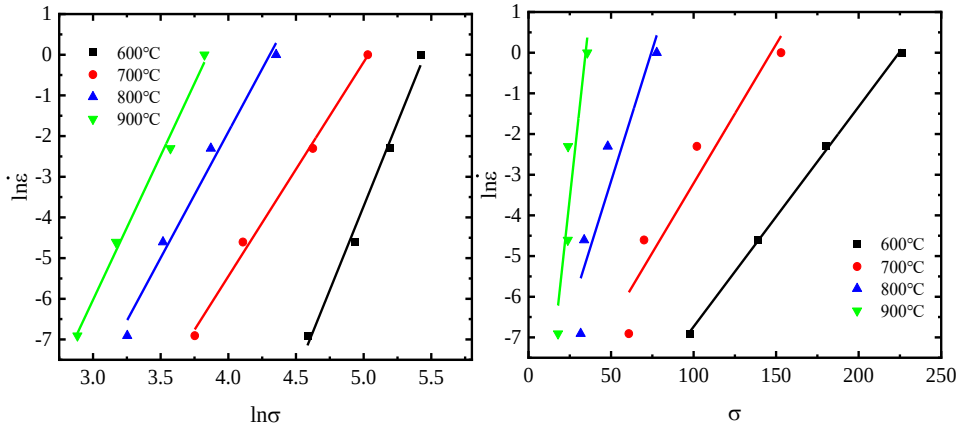

Figure 2. Relationship between flow stress and strain rate at different deformation temperatures for C61300 aluminum bronze

As shown in Figure 2, the experimental data were fitted using Eqs. (5) and (6), yielding the material constants $n_1 = 6.7000275$ and $\beta = 0.1561125$ from the slopes of the plots of $\ln\dot{\varepsilon} - \ln\sigma$ and $\ln\dot{\varepsilon} - \sigma$ respectively. Based on the relationship among, n_1, β and α, the parameter α was determined to be $\alpha = 0.023300277498861$. When the strain rate $\dot{\varepsilon}$ is a constant values, R, n, A and α are all constant. The activation energy for hot deformation Q, which varies with temperature, can be calculated by rearranging Eq.(3):

$$Q = Rn\left[\frac{\partial \ln\left[\sinh(\alpha\sigma)\right]}{\partial(1/T)}\right]_{\dot{\varepsilon}=cons\tan t} \tag{7}$$

$$\ln A = \ln\dot{\varepsilon} + \frac{Q}{RT} - n\ln\left[\sinh(\alpha\sigma)\right] \tag{8}$$

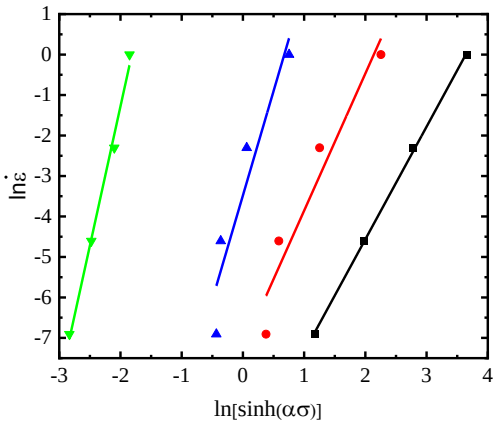

Figure 3. Arrhenius plot of ln $ln\dot{\varepsilon}$ versus [sinh($\alpha\sigma$)] for C61300 aluminum bronze

https://doi.org/10.64486/m.65.2.10

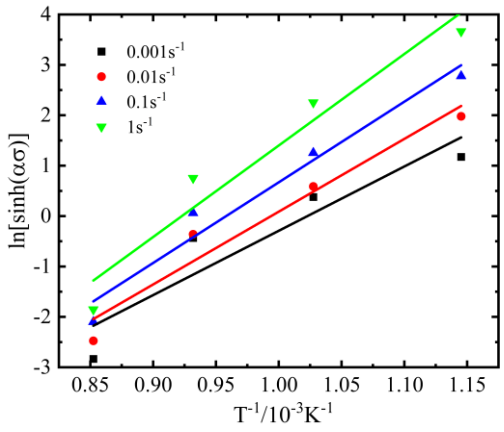

Figure 4. Linearized Arrhenius plot of ln[sinh($\alpha\sigma$)] versus 1/T for C61300 aluminum bronze at different strain rates.

As shown in Fig. 4 and Fig. 5, the material constants n and K were obtained by linear regression from the slopes of the fitted lines, giving $n = 4.5527575$ and $K = 15.3378975$. The activation energy Q was then calculated using the relationship $Q = nRK$ yielding $Q = 580564.35757233981$ J/mol. Using this value of Q, the intercept ln A was determined from the linear fit of $\ln A - Q/RT = -2.0867725013650238$, and the average value of the material constant A was obtained as $A = 1.6759 \times 10^{13}$.

In summary, for C61300 aluminium bronze under deformation temperatures (600–900) °C and strain rate (0.001–1) s^{-1} the constitutive equation can be expressed as:

$$\dot{\varepsilon} = 1.6759 \times 10^{33} \left[\sinh(0.023300277498861\sigma)\right]^{4.5527575} \exp\left(\frac{-580564.35757233981}{8.314T}\right) \quad (9)$$

4. Conclusions

C61300 aluminum bronze exhibits pronounced dynamic recovery and dynamic recrystallization during high-temperature compression deformation. The flow-stress curves show an initial work-hardening stage followed by a steady-state deformation stage. At a given deformation temperature, the flow stress increases with increasing strain rate, while at a fixed strain rate, the flow stress decreases with increasing temperature. A constitutive model based on the Arrhenius-type equation was developed by incorporating a temperature-compensated strain-rate parameter. Analysis and validation indicate that the predicted flow-stress values obtained from the proposed model show good agreement with the experimental results. Therefore, the model provides a useful theoretical basis for predicting and controlling the hot-deformation behavior of C61300 aluminum bronze and for optimizing its hot-working parameters. The findings offer practical guidance for the forming process of adjustable slide-rail components in gymnastics equipment.

References

[1] H. Zhou and K.-L. Ting, "Adjustable slider–crank linkages for multiple path generation," *Mechanism and Machine Theory*, vol. 37, no. 5, pp. 499–509, May 2002, https://doi.org/10.1016/S0094-114X(02)00008-3

[2] D. U. Khasyanova and M. A. Mukutadze, "The regularity of increasing the wear resistance of a modified radial slide bearing," *Journal of Machinery Manufacture and Reliability*, vol. 52, no. 2, pp. 151–160, Apr. 2023, https://doi.org/10.3103/S1052618823010065

[3] T. Herlambang, D. A. Fahmi, and U. H. Zhannisa, "Innovation of artistic gymnastics equipment in limited space," *Advance Sustainable Science Engineering and Technology*, vol. 7, no. 1, p. 02501025, Jan. 2025, https://doi.org/10.26877/asset.v7i1.1147

https://doi.org/10.64486/m.65.2.10

[4] G. Chapman *et al.*, "Biomechanical comparison of adjustable-loop femoral cortical suspension devices for soft tissue ACL reconstruction," *Orthopaedic Journal of Sports Medicine*, vol. 11, no. 2, p. 23259671221146788, Feb. 2023, https://doi.org/10.1177/23259671221146788

[5] Y. A. Kedir and H. G. Lemu, "Prediction of fatigue crack initiation under variable amplitude loading: Literature review," *Metals*, vol. 13, no. 3, p. 487, Feb. 2023, https://doi.org/10.3390/met13030487

[6] B. Leng *et al.*, "A critical review of anti-corrosion chemical surface treatment of aluminum alloys used for sports equipment," *Crystals*, vol. 14, no. 1, p. 101, Jan. 2024, https://doi.org/10.3390/cryst14010101

[7] F. Alkelae and S. Sasaki, "Tribological and mechanical characterization of nickel aluminium bronze manufactured by laser powder-bed fusion," *Tribology Online*, vol. 15, no. 3, pp. 126–135, May 2020, https://doi.org/10.2474/trol.15.126

[8] Z. Yue *et al.*, "Study on the dry fretting-sliding composite wear behavior of nickel–aluminum bronze," *Tribology International*, vol. 19, no. 7, p. 109802, Sep. 2024, https://doi.org/10.1016/j.triboint.2024.109802

[9] S. Ma *et al.*, "Effect of annealing temperature on microstructure and properties of a heavy warm rolled nickel aluminum bronze alloy," *Metallurgical and Materials Transactions A*, vol. 54, no. 1, pp. 293–311, Nov. 2023, https://doi.org/10.1007/s11661-022-06873-1

[10] L. Wang *et al.*, "A review on corrosion behavior and surface modification technology of nickel aluminum bronze alloys: Current research and prospects," *Advanced Engineering Materials*, vol. 27, no. 1, p. 2401779, Nov. 2025, https://doi.org/10.1002/adem.202401779

[11] R. D. Chauhan and P. K. Bharti, "A review of tribological excellence of bronze alloys," *Discover Applied Sciences*, vol. 7, no. 4, p. 283, Mar. 2025, https://doi.org/10.1007/s42452-025-06610-4

[12] S. Ma *et al.*, "Microstructure evolution during the heavy warm rolling of a nickel aluminum bronze," *Materials Science and Engineering: A*, vol. 883, p. 145458, Sep. 2023, https://doi.org/10.1016/j.msea.2023.145458

[13] R. Lu *et al.*, "Study of the mechanical properties and microstructure of spiral tubes and actuators for controlled extension fabricated with beryllium bronze strips," *Materials*, vol. 16, no. 20, p. 6719, Oct. 2023, https://doi.org/10.3390/ma16206719

[14] B.-B. Zhang *et al.*, "Tribocorrosion behavior of nickel aluminum bronze in seawater: Identification of corrosion–wear components and effect of pH," *Materials and Corrosion*, vol. 69, no. 1, pp. 106–114, Aug. 2017, https://doi.org/10.1002/maco.201709648

[15] M. R. da Silva *et al.*, "Copper alloys performance in high-pressure and low-velocity conditions using a custom tribometer," *Applied Sciences*, vol. 14, no. 14, p. 6001, Jul. 2024, https://doi.org/10.3390/app14146001

[16] F. Yang *et al.*, "The role of nickel in mechanical performance and corrosion behaviour of nickel–aluminium bronze in 3.5 wt.% NaCl solution," *Corrosion Science*, vol. 139, pp. 333–345, Jul. 2018, https://doi.org/10.1016/j.corsci.2018.05.012

[17] M. Roshan *et al.*, "A review on fatigue characteristics of nickel–aluminum bronze: Conventionally fabricated and additively manufactured," *Fatigue & Fracture of Engineering Materials & Structures*, vol. 48, no. 2, pp. 535–565, Nov. 2025, https://doi.org/10.1111/ffe.14499

[18] M. M. Quazi *et al.*, "Laser-based surface modifications of aluminum and its alloys," *Critical Reviews in Solid State and Materials Sciences*, vol. 41, no. 2, pp. 106–131, Feb. 2016, https://doi.org/10.1080/10408436.2015.1076716

[19] Y. Mu *et al.*, "Strengthening mechanism of mechanical properties of lightweight mullite fiber thermal insulation materials with different types of binders," *Ceramics International*, vol. 50, no. 11, pp. 18718–18728, Jun. 2024, https://doi.org/10.1016/j.ceramint.2024.02.360

[20] X. Cai *et al.*, "Experimental investigation on wear resistance and corrosion behavior of nickel–aluminum bronze alloy fabricated by wire-arc additive manufacturing," *Journal of Materials Research and Technology*, vol. 26, pp. 5801–5815, Oct. 2023, https://doi.org/10.1016/j.jmrt.2023.08.313

[21] Z.-t. Fu *et al.*, "Identification of constitutive model parameters for nickel aluminum bronze in machining," *Transactions of Nonferrous Metals Society of China*, vol. 26, no. 4, pp. 1105–1111, Apr. 2016, https://doi.org/10.1016/S1003-6326(16)64207-3

[22] S. Zeng *et al.*, "The constitutive relations and thermal deformation mechanism of nickel aluminum bronze," *Materials & Design*, vol. 220, p. 110853, Aug. 2022, https://doi.org/10.1016/j.matdes.2022.110853

[23] F. Cheng, S.-M. Kim, J. N. Reddy, and R. K. Abu Al-Rub, "Modeling of elastoplastic behavior of stainless-steel/bronze interpenetrating phase composites with damage evolution," *International Journal of Plasticity*, vol. 61, pp. 94–111, Oct. 2014, https://doi.org/10.1016/j.ijplas.2014.05.001

[24] H. Zhan *et al.*, "Research on mechanical properties and constitutive model of LYP160 steel after high temperature," *Structures*, vol. 76, p. 108943, Jun. 2025, https://doi.org/10.1016/j.istruc.2025.108943

.

https://doi.org/10.64486/m.65.2.10